Thermal fluctuations in metastable fluids

Cite as: Physics of Fluids (in press) (2022); https://doi.org/10.1063/5.0132478
Submitted: 28 October 2022 • Accepted: 26 November 2022 • Accepted Manuscript Online: 30 November 2022

Mirko Gallo

Accepted to Phys. Fluids 10.1063/5.0132478

Thermal fluctuations in metastable fluids

M. Gallo[1, a)]
School of Computing, Engineering and Mathematics, University of Brighton, Lewes Road, Brighton, UK

(Dated: November 25, 2022)

In this work, the thermal fluctuations of fluid in metastable conditions have been theoretically investigated. The fluid is described with a diffuse interface approach based on the Van der Waals squared-gradient theory (SGT), where the free energy is augmented by a density square gradient term to take into account capillary effects. By averaging physical observables on coarse-graining cells, it is found that capillarity strongly modifies the fluctuation statistics when increasing fluid metastability. A remarkable difference with respect to simple fluid description is also detected when approaching nanoscopic scales. Peculiarly, near spinodal loci, the classical theory envisages a divergent behavior of density fluctuations intensity, while the SGT provides a finite variance of the density field. The scaling behavior of density fluctuations near spinodal lines is analytically derived and discussed. Finally, the correlation length of the capillary system is identified for different metastabilities. Also in the latter case, the critical exponents are theoretically calculated. The theoretical results are corroborated by Landau-Lifshitz-Navier-Stokes fluctuating hydrodynamics simulations.

I. INTRODUCTION

At the mesoscale, even in equilibrium, thermal fluctuations play a relevant role. Below the micrometer scale, a continuum description should have the memory of matter granularity. Starting from the pioneering work of Einstein[1] several coarse-grained descriptions of fluids have been developed to take into account thermal noise in a continuum setting[2–8,9,10]. Landau and Lifshitz developed the "Fluctuating Hydrodynamics theory" for a simple one-component fluid, where the standard Navier-Stokes equations have been augmented with stochastic fluxes to take into account thermal fluctuations in hydrodynamics, the Landau-Lifshitz-Navier-Stokes equations (LLNS). In recent years there has been a substantial increase in numerical algorithms to perform *in-silico* experiments based on stochastic partial differential equations as LLNS[11–16]. These schemes are designed in order to capture the correct statistical properties of the fluctuating fields at a discrete level. From an experimental point of view, light scattering, X-ray diffraction, and neutron scattering have been used to measure static and dynamic structure factors[5,17]. Experiments are found to be in accordance with theoretical expectations. The study of thermal fluctuations is of pivotal importance for a plethora of physical phenomena. For instance, the modeling of thermal fluctuations is crucial in micro/nanoflows[1819–22], in the study of biological systems, such as lipid membranes[2324], for Brownian engines and molecular motors prototypes[25], and for reactive mixtures[26,27]. Molecular dynamics (MD) is a valuable tool to address these processes, however, its relevant computational cost limits the range of applicability to the nanoscale. In addition, the typical time scale of atom motion is significantly smaller than its hydrodynamic counterpart, resulting in the unenforceability of MD in some configurations of applicative interest. Therefore, the development of mesoscale descriptions is fundamental to addressing the full-scale dynamics of physical systems where the microscopic degree of freedoms (modeled as thermal fluctuations) influence the macroscopic scales. This is the case with multiscale phenomena where macroscopic physical observables are inherently interconnected with the microscopic ones. A relevant physical problem with the aforementioned features is the phase change in fluids, where the new phase originates at the atomistic levels and develops onto macroscopic (hydrodynamics) scales[28]. Another important example is the diffusion process of interfaces between miscible fluids. In fact, in non-equilibrium states, e.g. in presence of macroscopic concentration gradients, *giant fluctuations* can result due to a coupling between velocity and concentration fluctuations. This has been experimentally observed in micro-gravity experiments for a free diffusion process[29]. Recently it has been shown that thermal noise competes with turbulent fluctuations by modifying the turbulent kinetic energy spectrum[30–33]. For the description of such systems, it seems natural to develop mesoscale methods able to describe both the macroscopic scales of the fluid (slow variables of the physical system) and the effects of the microscopic degree of freedom (fast variables) modeled as stochastic processes. Clearly, the statistical description of thermal fluctuations is needed for the development of such mesoscale models.

The present work aims to identify the thermal fluctuation statistics of a capillary fluid in metastable conditions. A thermodynamically metastable state is represented by a local minimum of the free energy, separated by the stable one by an energy barrier. In that condition, the fluid can result in a "stable "state beyond the saturation conditions without experiencing the phase transformations. In fact, in that conditions, the phase change can occur with a certain probability (related to the degree of metastability) as a stochastic process, when the free energy barrier is surmounted due to thermal fluctuations. In particular, an intense fluctuation event, the so-called

a) m.gallo2@brighton.ac.uk

"rare event " in thermally activated processes, triggers the *incipit* of phase change nucleating an embryo of the new phase[3435]. In this respect, metastability can be seen as a thermodynamic stable state, with stability limited in time. In order to address this problem, the classical description of a one-component system (simple fluid) should be augmented to take into account additional energy contributions, e.g. capillarity and elasticity. In the context of phase transformations in fluids (condensations and vaporization), surface tension plays a fundamental role. In fact, the balance between volume forces (pressure difference expending work in the new phase formation) and the "elastic reaction " due to surface tension governs the phase transformation phenomenon[36]. Clearly, the surface tension penalizes the formation of new-phase regions and modifies the thermal noise spectrum.

In this paper, the statistical properties of thermal fluctuations for a capillary fluid in metastable conditions are theoretically investigated, both for the liquid and vapor phases. The fluid description is given in terms of the Van der Waals squared-gradient theory (SGT) for the Helmholtz free-energy functional[37]. Contrary to the usual thermodynamic description of simple fluids, where the fluid energy only depends on the local value of density and temperature fields, here a squared-gradient approximation of the free energy functional is used to describe the thermodynamic system

$$F[\rho,T]=\int_V f_b(\rho,T)+\frac{\lambda}{2}\boldsymbol{\nabla}\rho\cdot\boldsymbol{\nabla}\rho\,\mathrm{d}V\,, \tag{1}$$

with $f_b(\rho,T)$ the Helmholtz bulk free-energy density, given in terms of density and temperature fields, and λ is the capillary coefficient. The latter coefficient controls both the surface tension $\gamma\sim\lambda^{1/2}$ and the liquid/vapor interface thickness $\epsilon\sim\lambda^{1/2}$,[38]. Clearly, when $\lambda\to 0$, the classical description of one-component simple fluid is recovered.

The mesoscale description of the fluid dates back to Van der Waals[37] and can be formally derived from the density functional theory in the limit of small density gradient[39,40]. Despite its simple form, the model has proven to be an excellent descriptor of the physics of fluids at the mesoscale, correctly describing: the nucleation of droplets and bubbles[28,40–42], the stability limit of stretched water[43,44], evaporation and condensation processes[45–47], boiling phenomenon[48], cavitation collapse[38,49,50], droplet dynamics[51] and liquid films[52]. Recently diffuse interface-based models have been also developed to study topological transitions in lipid membranes[53] and reactive blending of polymers[54].

An extended comparison between the two fluid descriptions is performed, showing that the effect of capillarity strongly changes the statistical properties of density fluctuations when increasing the metastability of the fluid, or when approaching nanometric spatial scales (the typical length of liquid-vapor interface thickness). In particular, near spinodal conditions, the simple fluid theory leads to divergent behavior of density fluctuations, while the SGT provides a finite variance of the density field. Detailed analysis of the size of the coarse-graining cell size is also given, highlighting that for large enough coarse-graining volumes the effect of capillarity vanishes whether the metastability is low. The theoretical results are corroborated by fluctuating hydrodynamics simulations, both for LLNS and Capillary Landau-Lifshitz-Navier-Stokes (CLLNS). The latter set of equations represents the SGT version of a dynamical density functional theory[28,41,55–58]. The findings highlight the importance of considering capillarity when modeling metastable fluids or, more generally, in fluids at the nanoscale.

What follows is a schematic structure of the paper. In §II the fluctuations statistics of a capillary fluid are theoretically derived and compared with the ones predicted by the classical theory ($\lambda\to 0$). In order to streamline the narrative, some technical details are discussed in §A. In Sec §III the statistics of the fluctuations are discussed for metastable fluids, focusing on the density fluctuations behavior near spinodal loci as well as on the coarse-graining volume dependence of the density variances. In the latter section, the theoretical predictions are also compared with numerical simulation results. The numerical simulation details are given in §IV. Finally, §V underlines the main results of the work.

II. THEORY

For a fluid in equilibrium conditions, the fluctuation statistics of density $\rho(\mathbf{x})$, velocity $\mathbf{v}(\mathbf{x})$, and temperature $T(\mathbf{x})$ are related to the entropy deviation with respect to its maximum equilibrium value,[1]. For an isolated thermodynamic system, with constant mass M_0, volume V, and constant energy E_0, the entropy deviation functional can be written as

$$\begin{aligned}\tilde{\mathcal{S}}_{\,\lambda}[\tilde\rho,\tilde{\mathbf{v}},\tilde T]&=\mathcal{S}_\lambda[\rho,\mathbf{u},T]-\mathcal{S}_\lambda[\rho_0,\mathbf{0},T_0]\\&=\int_V s(\rho,T)-s(\rho_0,T_0)\,\mathrm{d}V+\\&+k_1\left(M_0-\int_V\rho\,\mathrm{d}V\right)\\&+k_2\left(E_0-\int_V\frac{1}{2}\rho\mathbf{v}\cdot\mathbf{v}+u_b\left(\rho,T\right)+\frac{1}{2}\lambda\boldsymbol{\nabla}\rho\cdot\boldsymbol{\nabla}\rho\,\mathrm{d}V\right),\end{aligned} \tag{2}$$

with $\tilde\rho=\rho-\rho_0$, $\tilde{\mathbf{v}}=\mathbf{v}$, $\tilde T=T-T_0$ the fluctuating fields, and, $\rho=\rho_0$, $T=T_0$, $\mathbf{v}=\mathbf{0}$ the fluid equilibrium states. Such states are found by imposing that the first variation of the functional in Eq. (2) is zero, i.e. $\delta\tilde{\mathcal{S}}_\lambda\left[\rho_0,\mathbf{0},T_0\right]=0$, where $s(\rho,T)$ and $u_b(\rho,T)$ are the bulk entropy and the internal energy densities, respectively. The functional maximization also leads to identifying the two Lagrange multipliers k_1 and k_2 enforcing mass and energy conservation. $k_1=-\mu_{c\,0}/T_0$, $k_2=1/T_0$, where $\mu_{c\,0}=\delta\tilde{\mathcal{S}}_\lambda/\delta\rho=\mu_b(\rho_0,T_0)-\lambda\nabla^2\rho_0$ is the equilibrium generalized chemical potential, $\mu_b=\partial u_b/\partial\rho-T\partial s/\partial\rho$ is the bulk chemical potential, and $\delta/\delta\rho$ is the functional derivative with respect to the density. Meaning that,

in equilibrium, the fluid mean temperature is constant, as well as the generalized chemical potential. For small fluctuations, the entropy functional can be expanded in a Taylor series around the equilibrium value

$$\tilde{\mathcal{S}}_\lambda[\tilde{\rho},\tilde{\mathbf{v}},\tilde{T}] \simeq \tilde{\mathcal{S}}_{\lambda 2}[\tilde{\rho},\tilde{\mathbf{v}},\tilde{T}] = \\ -\frac{1}{2}\int_V \mathrm{d}V \frac{c_{T0}^2}{T_0\rho_0}\tilde{\rho}^2 - \frac{\lambda}{T_0}\tilde{\rho}\left(\nabla^2\tilde{\rho}\right) + \frac{\rho_0}{T_0}\tilde{\mathbf{v}}\cdot\tilde{\mathbf{v}} + \frac{\rho_0 c_{v0}}{T_0^2}\tilde{T}^2, \tag{3}$$

where $c_{T0} = \partial p/\partial\rho|_T$ is the isothermal speed of sound, $p(\rho,T) = \rho\mu_b - f_b$ the bulk pressure and $c_{v0} = 1/\rho\,\partial s/\partial T|_\rho$ the specific heat at constant volume. The above equation can be rewritten in the form

$$\tilde{\mathcal{S}}_{\lambda 2}[\mathbf{\Delta}] = -\frac{1}{2}\int_V\int_V \mathbf{\Delta}(\mathbf{x})^\dagger \mathcal{H}_\lambda(\mathbf{x},\mathbf{y})\,\mathbf{\Delta}(\mathbf{y})\,\mathrm{d}V_x\,\mathrm{d}V_y\,, \tag{4}$$

where $\mathbf{\Delta} = (\tilde{\rho},\tilde{\mathbf{v}},\tilde{T})$ is the vector of the the fluctuating fields, $\mathbf{\Delta}^\dagger$ its adjoint, and $\mathcal{H}_\lambda$ is a diagonal, positive definite matrix operator

$$\mathcal{H}_\lambda = \begin{pmatrix} \frac{c_{T0}^2}{T_0\rho_0} - \frac{\lambda}{T_0}\nabla^2_{\mathbf{x}} & 0 & 0 \\ 0 & \frac{\rho_0}{T_0}\mathbf{I} & 0 \\ 0 & 0 & \frac{\rho_0 c_{v0}}{T_0^2} \end{pmatrix}\delta(\mathbf{x}-\mathbf{y})\,, \tag{5}$$

with $\mathbf{I}$ the 3×3 identity matrix, $\delta(\mathbf{x}-\mathbf{y})$ the Dirac delta function, and $\nabla^2_{\mathbf{x}}$ the Laplacian operator with respect to $\mathbf{x}$. Under these assumptions, the probability distribution functional for the fluctuating fields $\mathbf{\Delta}$ reads

$$P_{eq}[\mathbf{\Delta}] = \frac{1}{Z}\exp\left(\frac{\tilde{\mathcal{S}}_{\lambda 2}}{k_B}\right), \tag{6}$$

with k_B the Boltzmann constant, and Z the normalization constant. Hence the correlation tensor is

$$\mathbf{C}_\lambda(\mathbf{x},\mathbf{y}) = \langle \mathbf{\Delta}(\mathbf{x})\otimes\mathbf{\Delta}(\mathbf{y})^\dagger\rangle \\ = \frac{1}{Z}\int \mathcal{D}\mathbf{\Delta}\;\mathbf{\Delta}\otimes\mathbf{\Delta}^\dagger\exp\left(\frac{\tilde{\mathcal{S}}_{\lambda 2}}{k_B}\right), \tag{7}$$

where $\langle\rangle$ denotes the average operation, and it is evaluated in closed form by integrating the Gaussian path integrals[57]. The integration of Eq. 7 allows the reconstruction of the entire correlation tensor (see §A for derivation details)

$$\mathbf{C}_\lambda(\mathbf{x},\mathbf{y}) = k_B\mathcal{H}_\lambda^{-1}(\mathbf{x},\mathbf{y}) = \begin{pmatrix} C_{\lambda 11} & 0 & 0 \\ 0 & \mathbf{C}_{\lambda 22} & 0 \\ 0 & 0 & C_{\lambda 33} \end{pmatrix}, \tag{8}$$

with

$$C_{\lambda 11}(\mathbf{x}-\mathbf{y}) = \frac{\mathrm{k}_B T_0}{4\pi\lambda\,|\mathbf{x}-\mathbf{y}|}\exp\left(-|\mathbf{x}-\mathbf{y}|\sqrt{\frac{c_{T0}^2}{\rho_0\lambda}}\right), \tag{9}$$

$$\mathbf{C}_{\lambda 22}(\mathbf{x}-\mathbf{y}) = \langle\tilde{\mathbf{v}}(\mathbf{x})\otimes\tilde{\mathbf{v}}(\mathbf{y})\rangle = \frac{k_B T_0}{\rho_0}\mathbf{I}\delta(\mathbf{x}-\mathbf{y})\,, \tag{10}$$

$$C_{\lambda 33}(\mathbf{x}-\mathbf{y}) = \langle\tilde{T}(\mathbf{x})\tilde{T}(\mathbf{y})\rangle = \frac{k_B T_0^2}{\rho_0 c_{v0}}\delta(\mathbf{x}-\mathbf{y})\,. \tag{11}$$

The above results show that in the Gaussian approximation of the probability distribution functional, the equilibrium correlations for velocity and temperature fields are delta-correlated in space, while the capillary contribution to the free energy induces an exponential decay of the density correlation. In a simple fluid, where $\lambda = 0$, the entropy functional given in Eq. 3 reduces to

$$\tilde{\mathcal{S}}_{02}[\tilde{\rho},\tilde{\mathbf{v}},\tilde{T}] = \\ -\frac{1}{2}\int_V \mathrm{d}V\frac{c_{T0}^2}{T_0\rho_0}\tilde{\rho}^2 + \frac{\rho_0}{T_0}\tilde{\mathbf{v}}\cdot\tilde{\mathbf{v}} + \frac{\rho_0 c_{v0}}{T_0^2}\tilde{T}^2 \\ -\frac{1}{2}\int_V\int_V \mathbf{\Delta}(\mathbf{x})^\dagger\mathcal{H}_0(\mathbf{x},\mathbf{y})\,\mathbf{\Delta}(\mathbf{y})\,\mathrm{d}V_x\,\mathrm{d}V_y \tag{12}$$

with

$$\mathcal{H}_0 = \lim_{\lambda\to 0}\mathcal{H}_\lambda = \begin{pmatrix} \frac{c_{T0}^2}{T_0\rho_0} & 0 & 0 \\ 0 & \frac{\rho_0}{T_0}\mathbf{I} & 0 \\ 0 & 0 & \frac{\rho_0 c_{v0}}{T_0^2} \end{pmatrix}\delta(\mathbf{x}-\mathbf{y}) \tag{13}$$

whose expression is also reported in[2,5], where the fluctuation statistics of a simple fluid are discussed. In particular, the classical theory provides that the velocity and temperature fields have the same correlation functions as in the present case (see Eq.s 10, 11), i.e. $\mathbf{C}_{022} = \mathbf{C}_{\lambda 22}, C_{033} = C_{\lambda 33}$. This can be easily deduced since, $\mathbf{C}_\lambda = k_B\mathcal{H}_\lambda^{-1}$, hence $\mathbf{C}_0 = k_B\mathcal{H}_0^{-1}$. By recognizing that $\mathcal{H}_{\lambda 22} = \mathcal{H}_{022}$ and $\mathcal{H}_{\lambda 33} = \mathcal{H}_{033}$ one realizes that $\mathbf{C}_{022} = \mathbf{C}_{\lambda 22}, C_{033} = C_{\lambda 33}$.

It is worth stressing that the second-order expansion of the entropy functional (Eq. 4) depends on λ only through the density field, meaning that capillarity only affects the density fluctuation statistics. In fact, when $\lambda \to 0$ the density field variance differs from the Eq.(9), taking the form

$$C_{011}(\mathbf{x}-\mathbf{y}) = k_B\mathcal{H}_{011}^{-1}(\mathbf{x}-\mathbf{y}) = \frac{k_B T_0\rho_0}{c_{T0}^2}\delta(\mathbf{x}-\mathbf{y})\,. \tag{14}$$

Since the statistical properties of velocity and temperature fields are not affected by the squared-gradient approximation of the fluid free energy, this work will focus on the role of the capillary effects on the density fluctuations.

III. RESULTS AND DISCUSSIONS

In Fig.1 the pressure field $p(\rho,T)$ for a homogeneous fluid is reported as a function of the mean density field

Accepted to Phys. Fluids 10.1063/5.0132478

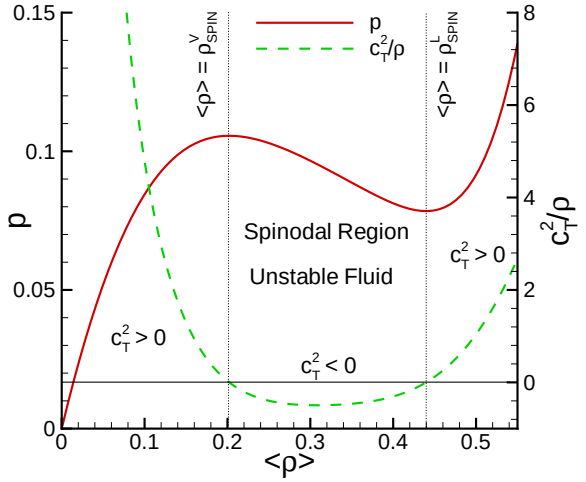

Figure 1. The red solid line represents the pressure (p) as a function of the mean density $\langle\rho\rangle$ for a Lennard-Jones EoS[59]. The isotherm $T = 1.25$ is considered. The dotted green line depicts the squared isothermal speed of sound normalized with the density field (c_T^2/ρ). The other two vertical curves, dotted black lines, indicate the liquid ($\langle\rho\rangle = 0.4397$) and vapor ($\langle\rho\rangle = 0.2021$) spinodal densities. They are identified on the isotherm where $\partial p/\partial\rho|_T = c_T^2 = 0$. The density values comprised between the spinodal ones characterize an unstable fluid, where the isothermal speed of sound becomes a complex number.

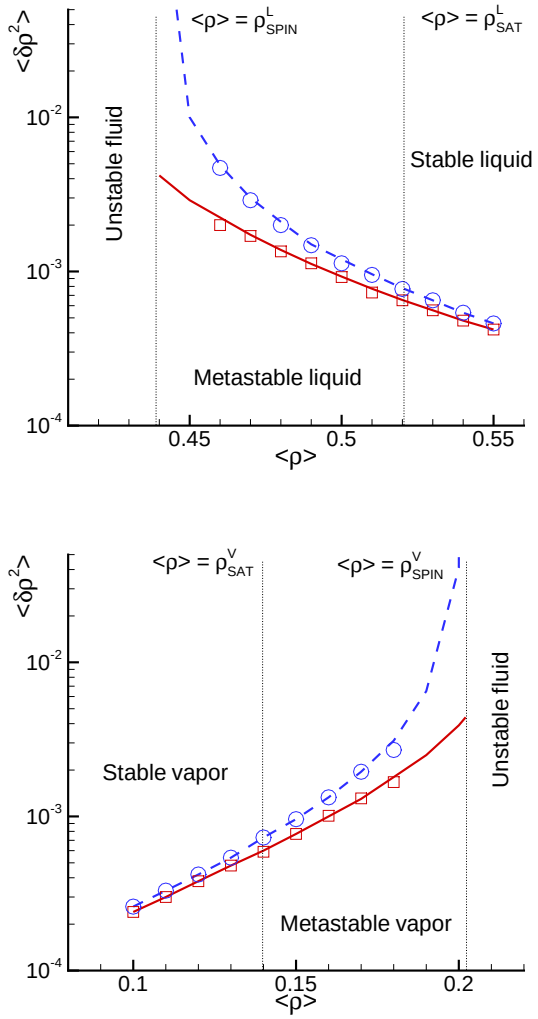

Figure 2. Top panel: Liquid phase density fluctuation variances averaged on a volume $V = 1000\sigma^3$ vs the density equilibrium value at $\langle T\rangle = 1.25$. The red solid line represents the square gradient theoretical prediction, the blue dotted curve depicts its counterpart for a simple fluid. The symbols identify the numerical results of fluctuating hydrodynamics equations. Red squares: CLLNS. Blue circles: LLNS. The density variance is evaluated for a stable liquid, $\rho \geq \rho_L^{SAT} = 0.5118$, for a metastable state, $\rho \in (\rho_L^{SPIN}, \rho_L^{SAT})$; in the unstable region the density fluctuations are not defined. Bottom panel: Vapor phase density fluctuation variances averaged on the same volume as in the liquid case, the equilibrium temperature is $\langle T\rangle = 1.25$. Lines and symbols reflect the same logic of the top panel. The density variance is evaluated for a stable vapor, $\rho \leq \rho_V^{SAT} = 0.1394$, for a metastable state, $\rho \in (\rho_V^{SAT}, \rho_V^{SPIN})$.

(red solid line). The adopted equation of state (EoS) is the Benedict-Webb-Rubin[59], mimicking a Lennard-Jones Fluid. p is made dimensionless with the reference pressure: $p_{ref} = e/\sigma^3$, where $\sigma = 3.4 \times 10^{-10} m$ and $e = 1.65 \times 10^{-21}\, J$. The density field is dimensionalized with the reference density $\rho_{ref} = m/\sigma^3$, with $m = 6.63 \times 10^{-26}$ Kg. The capillary coefficient is fixed as $\lambda = 5.224$, with its reference value as $\lambda_{ref} = \sigma^5 e/m^2$, to reproduce surface tension value obtained through Monte Carlo simulations[57]. The green dotted line, represents the isothermal speed of sound, $c_T^2 = \partial p/\partial\rho|_T$, normalized with the density. The latter quantity is positive in the stable regime and is negative in the unstable one, furthermore near the spinodal region $c_T^2 \to 0$ leading to a divergent behavior on the density fluctuations when $\lambda \to 0$, see Eq.s (14). Clearly, when considering metastable fluids, where the mean density value is comprised between the saturation density $\rho_{L/V}^{SAT}$ and the spinodal one $\rho_{L/V}^{SPIN}$, the intensity of density fluctuations is strongly different from the stable conditions.

In Fig.2, the variance of density fluctuations is reported for different thermodynamic conditions. Starting from the stable state, up to near spinodal conditions. The top panel depicts the fluctuations of the liquid phase, while the bottom one represents a vapor. The blue dotted lines are the theoretical predictions for a simple fluid ($\lambda = 0$), and the red continuum curves illustrate the squared-gradient theory. The theoretical predictions are compared to fluctuating hydrodynamics simulations, both for simple LLNS, and for CLLNS, see §IV for details. Numerical results are indicated with blue circles when considering simple LLNS, and with red squares for CLLNS

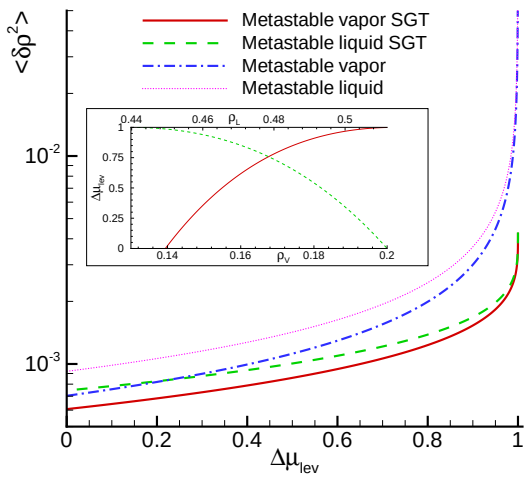

Figure 3. Density fluctuation variances as a function of the metastability level $\Delta\mu_{lev}$. The average volume is $V = 1000\sigma^3$, the equilibrium temperature is $\langle T\rangle = 1.25$. The red solid line and the green dashed curve indicate the square gradient prediction for the vapor and liquid phases, respectively. The dashed-dotted blue line (vapor) and the dotted purple one (liquid) depict the theoretical prediction for a simple fluid. Inset: the metastability level is reported as a function of liquid (red solid line) and vapor (green dashed line) densities.

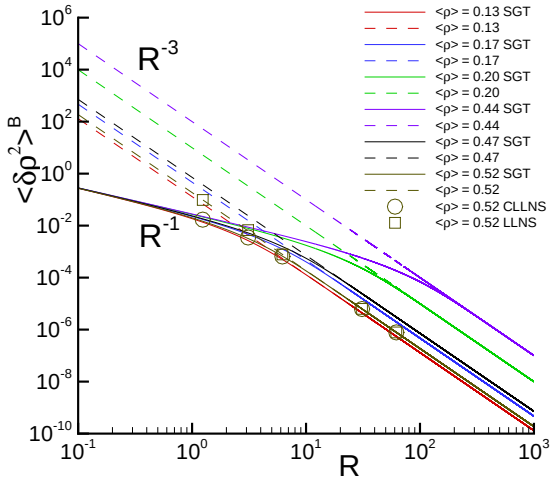

Figure 4. Variance of the density fluctuations ($\langle\delta\rho^2\rangle^{\mathcal{B}}$) averaged on a ball of radius R. The solid lines depict the square gradient theoretical values (SGT), while the dotted ones represent the theoretical prediction for a simple fluid, where $\lambda = 0$. The different colors refer to different mean density equilibrium values. The symbols identify the numerical values as obtained by fluctuating hydrodynamics simulations. Circles: CLLNS. Squares: LLNS.

cases. The theoretical values are directly derived from Eq.s (9,14), by considering an averaged value of the density on a fluid volume ΔV, as $\delta\rho = (\Delta V)^{-1}\int_{\Delta V}\tilde{\rho}(\mathbf{x})\,dV$, leading to

$$\langle\delta\rho^2\rangle_0 = \frac{1}{\Delta V}\int_{\Delta V} C_{011}\,dV \quad \langle\delta\rho^2\rangle_\lambda = \frac{1}{\Delta V}\int_{\Delta V} C_{\lambda 11}\,dV\,. \tag{15}$$

It is worthwhile noting that, the volume ΔV over which the fluctuating fields are averaged has the physical meaning of the coarse graining cell, that can be seen as an open system composed with a fluctuating number of molecules. At a mesoscopic level, this microscopic system is effectively modeled as the mean value of some relevant fields, like e.g. the density, and a stochastic process having the same statistical properties of the coarse grained field $(\delta\rho(\Delta V))$.

The first integral in Eq. (15) can be easily evaluated due to the delta-correlated form of density fluctuations when $\lambda = 0$, $\langle\delta\rho^2\rangle_0 = k_B T_0\rho_0/(c^2_{T0}\Delta V)$, the second one can be numerically estimated. The cell volume $V = \Delta x^3 = (10\sigma)^3$ is adopted, with the mean equilibrium temperature as $\langle T\rangle = 1.25$. The spatial scale Δx is chosen to be the nominal liquid/vapor interface thickness, which at this temperature is $\epsilon \simeq 10\sigma$. As evident from the two panels of Fig.(2) the more the fluid is metastable, the more density fluctuations increase, furthermore, the squared-gradient approximation of the fluid energy strongly changes the variances of thermal fluctuations. Specifically, capillarity reduces the intensity of fluctuations, since the surface tension penalizes the formation of low-high/density regions, in other terms $\lambda/2|\boldsymbol{\nabla}\rho|^2$ in Eq. (1) disadvantages the presence of density heterogeneity. Therefore, $\langle\delta\rho^2\rangle_\lambda < \langle\delta\rho^2\rangle_0$, with an increasing difference towards the spinodal limits. This difference culminates near the spinodal curves, where $\langle\delta\rho^2\rangle_0 \to \infty$, while $\langle\delta\rho^2\rangle_\lambda$ converges. The fluctuations behavior near spinodal can be directly determined in the case of $\lambda = 0$, by expanding c_T^2 around liquid/vapor spinodal densities

$$c_T^2\left(\rho_{L/V}^{SPIN}\right) \sim \frac{\partial^2 p}{\partial\rho^2}|_{\rho_{L/V}^{SPIN}}\left(\langle\rho\rangle - \rho_{L/V}^{SPIN}\right)\,, \tag{16}$$

leading to

$$\lim_{\langle\rho\rangle\to\rho_{L/V}^{SPIN}} \frac{\langle\delta\rho^2\rangle_0}{|\langle\rho\rangle - \rho_{L/V}^{SPIN}|^\alpha} = \ell_1(\langle T\rangle) < \infty\,, \tag{17}$$

when $\langle T\rangle < T_{CRIT}$, and $\alpha = -1$, with $T_{CRIT} = 1.33$, the critical temperature of the considered fluid. Hence, both for vapor and liquid phase, near spinodal conditions, the density fluctuations diverge with a "critical" exponent $\alpha = -1$

$$\langle\delta\rho^2\rangle_0 \sim |\langle\rho\rangle - \rho_{L/V}^{SPIN}|^{-1}\,. \tag{18}$$

Although the result is obtained for the adopted Benedict-Webb-Rubin EoS, it is expected to be general under the hypothesis that $\partial^2 p/\partial\rho^2|_{\rho_{L/V}^{SPIN}} \neq 0$ (thermodynamic stability for sub-critical fluids). In fact, when $T < T_{CRIT}$,

the pressure field around the spinodal lines is

$$p - p^{SPIN} \sim \frac{1}{2}\frac{\partial^2 p}{\partial \rho^2}|_{\rho^{SPIN}_{L/V}} \left(\langle\rho\rangle - \rho^{SPIN}_{L/V}\right)^2 \qquad (19)$$

coherently with Eq. 16.

In stable fluids, the classical description and the SGT are fairly in accordance. The difference is instead remarkable in metastable states. To quantify this discrepancy, let us introduce the metastability level $\Delta\mu_{lev} = (\mu_c - \mu^{SAT}_{cL/V})/(\mu^{SPIN}_{cL/V} - \mu^{SAT}_{cL/V})$ which is an important parameter characterizing how metastable a fluid is[60]. The latter quantity takes values in the set $[0, 1]$, with $\Delta\mu_{lev} \to 0$ when $\langle\rho\rangle \to \rho^{SAT}_{L/V}$ and $\Delta\mu_{lev} \to 1$ when $\langle\rho\rangle \to \rho^{SPIN}_{L/V}$, for liquids and vapors, respectively. The inset in Fig.(3) reports the values of the parameter $\Delta\mu_{lev}$ as a function of the mean density value. The red curve represents the vapor phase, while the green line illustrates the liquid state. In the main panel, the variance of the density fluctuations is reported as a function of the metastability level, metastable liquid and vapor are discussed. As evident in the entire metastable range, the SGT provides a relevant correction to the density variance when increasing the degree of metastability. Again, near spinodal loci ($\Delta\mu_{lev} \sim 1$) the classical theory of fluctuations provides a fluctuations divergence.

As discussed above, the scaling law of the density fluctuations divergence as a function of the metastability level can be inferred with by expanding the bulk chemical potential around the spinodal densities

$$\mu_{cL/V} - \mu^{SPIN}_{cL/V} \sim \frac{1}{2\rho}\frac{\partial^2 p}{\partial \rho^2}|_{\rho^{SPIN}_{L/V}} \left(\langle\rho\rangle - \rho^{SPIN}_{L/V}\right)^2 , \quad (20)$$

where the thermodynamic identity $\partial p/\partial\rho = \rho\partial\mu_c/\partial\rho$ has been invoked. Please noting that, the above approximation is again universal under the hypothesis $T < T_{CRIT}$ and $\partial^2 p/\partial\rho^2|_{\rho^{SPIN}_{L/V}} \neq 0$. Hence

$$\lim_{\Delta\mu_{lev}\to 1} \frac{\langle\delta\rho^2\rangle_0}{|1-\Delta\mu_{lev}|^\beta} = \ell_2(\langle T\rangle) < \infty , \qquad (21)$$

with $\beta = 1/2$, leading to

$$\langle\delta\rho^2\rangle_0 \sim |1-\Delta\mu_{lev}|^{-1/2} . \qquad (22)$$

In order to infer the square gradient correction to the density fluctuations near spinodal regions, let us consider the density average on a ball $\mathcal{B}(R)$ of radius R, $\langle\delta\rho\rangle^{\mathcal{B}} = 3/(R^3)\int_0^R \tilde{\rho}(r) r^2 dr$, its variance is given by

$$\langle\delta\rho^2\rangle^{\mathcal{B}}_\lambda = \frac{3}{4\pi R^3}\int_0^R C^\lambda_{11}(r) 4\pi r^2 \mathrm{d}r = \qquad (23)$$
$$= \langle\delta\rho^2\rangle^{\mathcal{B}}_0 \left[1 - \exp\left(-R\sqrt{\frac{c^2_{T0}}{\lambda\rho_0}}\right)\left(1 + R\sqrt{\frac{c^2_{T0}}{\lambda\rho_0}}\right)\right] ,$$

with $\langle\delta\rho^2\rangle^{\mathcal{B}}_0 = 3k_B T_0\rho_0/(4\pi c^2_{T0}R^3)$ is the spherically averaged variance in the case of $\lambda = 0$. At fixed R, it is easy to realize that, when $c^2_{T0} \sim 0$, one has

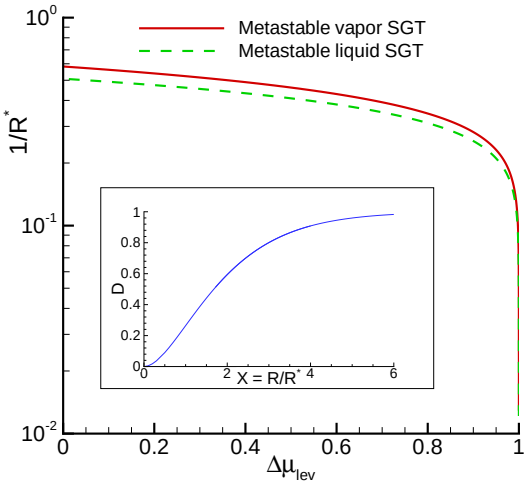

Figure 5. Behavior of the inverse of the reference capillary length ($1/R^*$) as a function of the metastability level ($\Delta\mu_{lev}$). The red solid line corresponds to the vapor phase, while the green dashed curve depicts the liquid state. In the inset the function $\mathcal{D} = \langle\delta\rho^2\rangle_\lambda/\langle\delta\rho^2\rangle_0$ as a function of the reduced radius $X = R/R^*$ is reported.

$$\langle\delta\rho^2\rangle^{\mathcal{B}}_\lambda \sim \frac{3k_B T_0}{8\pi\lambda R} , \qquad (24)$$

hence, near spinodal conditions, the density fluctuations are only controlled by the capillary coefficient and the mean temperature of the system. In addition, also the scaling with the averaging volume is different, whereas the SGT provides scaling of density fluctuations as $\langle\delta\rho^2\rangle^{\mathcal{B}}_\lambda \sim R^{-1}$, instead of $\langle\delta\rho^2\rangle^{\mathcal{B}}_0 \sim R^{-3}$ as predicted for simple fluids. In Fig.4 the spherically averaged variance of the density fluctuations ($\langle\delta\rho^2\rangle^{\mathcal{B}}$) is reported for different thermodynamic conditions as a function of the ball radius R. As in the previous figures, the classical theory and the SGT are depicted. What immediately stands out from the figure is the double scaling of the variance of thermal fluctuations as predicted by the SGT. Specifically, for small values of R, one has $\langle\delta\rho^2\rangle^{\mathcal{B}}_\lambda \sim R^{-1}$, whereas for large values of R the two different theories predict the same scaling as $\langle\delta\rho^2\rangle^{\mathcal{B}}_\lambda \sim \langle\delta\rho^2\rangle^{\mathcal{B}}_0 \sim R^{-3}$. Between the two regimes predicted by SGT, a transition zone can be seen, whose amplitude is dictated by the degree of fluid metastability. In fact, both for liquids and vapors, for high levels of metastability ($\langle\rho\rangle^{\mathcal{B}} \sim \rho^{SPIN}_{L/V}$) the scaling of the classical theory is achieved when considering radii of the order of hundreds of reduced lengths. Clearly, as discussed before, when $\rho \to \rho^{SPIN}_{L/V}$ the extension of the transition zone diverges, see Eq. (24). It is worth noting that for very small radii $R = \mathcal{O}(1)$, where the theory of fluctuating hydrodynamics is at the limit of applicability, the SGT predicts values of density fluctuation stably below the mean value of the field. Instead,

the classical theory leads to very large and unphysical fluctuations. Again, the aforementioned behavior is exacerbated by increasing metastability. In Fig. 4 are also reported the numerical simulation results of fluctuating hydrodynamics simulations, both for simple LLNS (army green squares) and for CLLNS (army green circles). The agreement is remarkable for all the analyzed cases.

Eq. (23), naturally introduce a physical length $R^* = [(\rho_0\lambda)/(c_T^2)]^{1/2}$, a reference capillary length (correlation length) related to the capillary coefficient and to the isothermal speed of sound. This quantity strongly depends on fluid thermodynamic conditions. In fact, since the capillary coefficient is identified by the surface tension, R^* varies with the metastability degree of the fluid (see Fig. 1 to visualize the behavior of c_T^2/ρ_0). In the main plot of Fig. 5 the inverse of R^* is reported as a function of the metastability level $\Delta\mu_{lev}$, for vapor (red solid line) and liquid (green dashed line) phases. For both liquid and vapor states, R^* is an increasing function of the metastability level, with $R^* \to \infty$ when $\Delta\mu_{lev} \to 1$. As discussed in the previous part of the section, the scaling behavior of R^* near spinodal loci can be easily deduced since $R^* \sim 1/c_T$ and $c_T \sim (\rho - \rho_{L/V}^{SPIN})^{1/2}$ (see Eq. 16), thus

$$R^* \sim |\langle\rho\rangle - \rho_{L/V}^{SPIN}|^{-1/2} \qquad R^* \sim |1 - \Delta\mu_{lev}|^{-1/4}\,. \quad (25)$$

This peculiar behavior is similar to what is observed in critical phenomena when approaching the critical temperature where the correlation length goes to infinity as well as the fluid compressibility, like e.g. *critical opalescence*. In addition, the critical exponent as predicted by the mean field approximation[61] when $T \to T_{CRIT}$ for the compressibility ($\mathrm{k}_T \sim |T - T_{CRIT}|^{-1}$) and for the correlation length ($R^* \sim |T - T_{CRIT}|^{-1/2}$) correspond to the present case when $\rho \to \rho_{L/V}^{SPIN}$.

Since R^* plays a decay length role, in highly metastable fluids the scaling of thermal fluctuations is only dominated by capillarity effects, consistently with Eq. (24). After introducing R^*, Eq. (23) also suggests to introduce a rescaled length variable $X = R/R^*$, and the ratio $\mathcal{D}(X)$ defined as

$$\mathcal{D} = \frac{\langle\delta\rho^2\rangle_\lambda^{\mathcal{B}}}{\langle\delta\rho^2\rangle_0^{\mathcal{B}}} = 1 - (1+X)\exp(-X)\,. \quad (26)$$

The function $\mathcal{D}(X)$ represents the ratio between the SGT prediction of the density fluctuations variance and its classical counterpart. This report condenses information about the level of metastability, the capillarity of the fluid, and the extent of the fluid volume over which we are averaging fluctuations. In the inset of Fig. 5, $\mathcal{D}(X)$ has been reported, showing that for $X > 5-6$ one has $\mathcal{D} \sim 1$, meaning that the capillary effects do not influence the variance of density fluctuations, hence recovering the classical theory. It is worth stressing that, given the specific thermodynamic condition of the fluid, and the capillary coefficient (surface tension) the curve $\mathcal{D}(X)$ can be univocally identified.

IV. NUMERICAL SIMULATIONS

Numerical simulations are conducted by solving the Landau-Lifshitz-Navier-Stokes equations both with capillary stresses ($\lambda \neq 0 \to$ CLLNS) and for a simple fluid where capillarity is omitted ($\lambda = 0 \to$ LLNS). The equations describe the balance for mass, momentum, and energy, augmented with stochastic thermodynamic fluxes.

$$\begin{aligned}
\frac{\partial\rho}{\partial t} + \boldsymbol{\nabla}\cdot(\rho\mathbf{u}) &= 0\,, \quad (27)\\
\frac{\partial\rho\mathbf{u}}{\partial t} + \boldsymbol{\nabla}\cdot(\rho\mathbf{u}\otimes\mathbf{u}) &= -\boldsymbol{\nabla}p + \boldsymbol{\nabla}\cdot\boldsymbol{\Sigma}_\lambda + \boldsymbol{\nabla}\cdot\boldsymbol{\delta\Sigma}\,,\\
\frac{\partial E}{\partial t} + \boldsymbol{\nabla}\cdot(\mathbf{u}E) &= \boldsymbol{\nabla}\cdot(-p\mathbf{u} + \mathbf{u}\cdot\boldsymbol{\Sigma}_\lambda - \mathbf{q}) +\\
&\quad + \boldsymbol{\nabla}\cdot(\mathbf{u}\cdot\boldsymbol{\delta\Sigma} - \boldsymbol{\delta q})\,,
\end{aligned}$$

where the symbol $\otimes$ denotes the tensor product. Concerning the deterministic fluxes, non-equilibrium thermodynamic arguments lead to the following expressions[41]

$$\begin{aligned}
\boldsymbol{\Sigma}_\lambda &= \left[\frac{\lambda}{2}|\boldsymbol{\nabla}\rho|^2 + \rho\boldsymbol{\nabla}\cdot(\lambda\boldsymbol{\nabla}\rho)\right]\boldsymbol{I} - \lambda\boldsymbol{\nabla}\rho\otimes\boldsymbol{\nabla}\rho + \quad (28)\\
&\quad + \mu\left[(\boldsymbol{\nabla}\mathbf{u} + \boldsymbol{\nabla}\mathbf{u}^T) - \frac{2}{3}\boldsymbol{\nabla}\cdot\mathbf{u}\boldsymbol{I}\right]\,,\\
\boldsymbol{q}_\lambda &= \lambda\rho\boldsymbol{\nabla}\rho\boldsymbol{\nabla}\cdot\mathbf{u} - k\boldsymbol{\nabla}T\,,
\end{aligned}$$

clearly, the standard description of the Newton-Fourier laws is recovered when $\lambda \to 0$.

$$\begin{aligned}
\boldsymbol{\Sigma}_0 &= \mu\left[(\boldsymbol{\nabla}\mathbf{u} + \boldsymbol{\nabla}\mathbf{u}^T) - \frac{2}{3}\boldsymbol{\nabla}\cdot\mathbf{u}\boldsymbol{I}\right]\,, \quad (29)\\
\boldsymbol{q}_0 &= -k\boldsymbol{\nabla}T\,.
\end{aligned}$$

The transport coefficients μ, k, represent the fluid viscosity and thermal conductivity of the LJ fluid.

The fluctuation-dissipation balance provides an explicit form of the stochastic fluxes[41]

$$\begin{aligned}
\langle\boldsymbol{\delta q}(\hat{x},\hat{t})\rangle &= 0\,, \quad (30)\\
\langle\boldsymbol{\delta\Sigma}(\hat{x},\hat{t})\rangle &= 0\,,\\
\langle\boldsymbol{\delta\Sigma}(\hat{x},\hat{t})\otimes\boldsymbol{\delta\Sigma}^\dagger(\tilde{x},\tilde{t})\rangle &= \mathbf{Q}^{\boldsymbol{\Sigma}}\delta(\hat{x}-\tilde{x})\delta(\hat{t}-\tilde{t})\,,\\
\langle\boldsymbol{\delta q}(\hat{x},\hat{t})\otimes\boldsymbol{\delta q}^\dagger(\tilde{x},\tilde{t})\rangle &= \mathbf{Q}^{\mathbf{q}}\delta(\hat{x}-\tilde{x})\delta(\hat{t}-\tilde{t})\,,
\end{aligned}$$

where

$$\begin{aligned}
\mathbf{Q}^{\boldsymbol{\Sigma}}{}_{\alpha\beta\nu\eta} &= 2\mathrm{k}_B T\mu(\delta_{\alpha\nu}\delta_{\beta\eta} + \delta_{\alpha\eta}\delta_{\beta\nu} - \frac{2}{3}\delta_{\alpha\beta}\delta_{\nu\eta})\,, \quad (31)\\
\mathbf{Q}^{\mathbf{q}}{}_{\alpha\beta} &= 2\mathrm{k}_B T^2 k\delta_{\alpha\beta}\,,
\end{aligned}$$

δ the Kronecker symbol, and $\delta\Sigma^\dagger$, $\delta q^\dagger$ the adjoint of the stochastic fluxes. Please note that for both LLNS and CLLNS the stochastic fluxes have the same expression. This is related to the fact that the capillary forces have a reversible nature, thus they do not produce entropy and, as a consequence, they do not alter the fluctuation-dissipation balance.

In numerical experiments, all quantities are made dimensionless following reference quantities: $L_{ref} = \sigma =$

$3.4 \times 10^{-10}\, m$ as length, $E_{ref} = e = 1.65 \times 10^{-21}\, J$ as energy, $T_{ref} = \epsilon/k_B$ as temperature, $m = 6.63 \times 10^{-26}\, Kg$ as mass, $U_{ref} = \sqrt{\epsilon/m}$ as velocity, $t_{ref} = L_{ref}/U_{ref}$ as time. The non-dimensional capillary coefficient is fixed as $\lambda = 5.224$, with its reference value as $\lambda_{ref} = \sigma^5 e/m^2$, see[57] for additional details. The equations of motion are solved with the method of lines. Concerning spatial discretization, a staggered central finite differences have been adopted. This method is particularly suitable when dealing with stochastic equations since it preserves at a discrete level, the continuum properties of the involved differential operators[13]. The temporal integration is conducted with a second-order explicit Runge-Kutta method. All the simulations are three-dimensional with $50 \times 50 \times 50$ numerical cells, with periodic boundary conditions. The adopted numerical time step (non-dimensional) is $\Delta t = 0.1$.

The numerical mean value of a generic observable $\mathcal{O}$

$$\langle \mathcal{O} \rangle = \frac{1}{N_t} \frac{1}{N_c} \sum_{i=1}^{N_t} \sum_{j=1}^{N_c} \mathcal{O}_j^i \,, \tag{32}$$

where $\mathcal{O}_j^i$ is the value of the observable $\mathcal{O}$ in the $j-th$ cell at the time i. $N_c = 50^3$ is the total number of numerical cells, and $N_t = 10^3$ is the number of independent time instants taken in the simulations. The total simulation time is $T = 10^5$.

V. CONCLUSIONS

In summary, the mesoscopic Van der Waals SGT has been employed to theoretically estimate the thermal fluctuation statistics of metastable fluids. The theory augments the classical thermodynamic description of simple fluids where fluid energy only depends on the local value of density and temperature. The SGT free energy modifies the structure of the entropy functional, resulting in a different fluctuation spectrum, which is analytically derived in closed form. By averaging the relevant statistical observables on coarse-graining volumes, it is found that capillarity plays a relevant role in metastable fluids, or when approaching nanometric scales. Peculiarly, near spinodal states, the classical theory leads to divergent behavior of density fluctuations intensity, while the SGT provides a finite variance of the density field. For the simple fluid, the scaling behavior of the density variance as a function of density and chemical potential is derived. Finally, the SGT gives access to the capillary correlation length, also in this case its scaling behavior is discussed for different metastabilities. The theoretical results are validated by fluctuating hydrodynamics numerical simulations. The presented results highlight the importance of considering capillarity in metastable fluids or, more generally, in fluids at the nanoscale.

VI. ACKNOWLEDGEMENTS

The author wants to acknowledge Carlo Massimo Casciola for the fruitful discussion on the work.
Support is acknowledged from DECI 17 SOLID project for resource Navigator based in Portugal at https://www.uc.pt/lca/ from the PRACE aisbl; CINECA award under the ISCRA initiative, for the availability of high-performance computing resources and support (ISCRA-B FHDAS).

VII. DECLARATION OF INTERESTS

The author report no conflict of interest.

Appendix A: Evaluation of the correlation tensor

In the following appendix, the evaluation of the correlation tensor for a Gaussian probability distribution functional is retraced, although the explicit calculation has been addressed in some past works[41,57], the main elements of the procedure are here reported for the reader's convenience.

The second-order approximation of the probability equilibrium distribution in Eq. 6 takes the form

$$P[\boldsymbol{\Delta}] = \frac{1}{Z} \exp\left(-\frac{1}{2k_B} \int_V \int_V \boldsymbol{\Delta}(\mathbf{x})^\dagger \mathcal{H}_\lambda(\mathbf{x},\mathbf{y})\, \boldsymbol{\Delta}(\mathbf{y})\, \mathrm{d}V_x\, \mathrm{d}V_y \right) , \tag{A1}$$

where the operator $\mathcal{H}_\lambda(\mathbf{x},\mathbf{y})$ is diagonal and positive definite operator defined in Eq. 13, and Z the normalization constant defined as

$$Z = \int \mathcal{D}\boldsymbol{\Delta}\, \exp\left(-\frac{1}{2k_B} \int_V \int_V \boldsymbol{\Delta}(\mathbf{x})^\dagger \mathcal{H}_\lambda(\mathbf{x},\mathbf{y})\, \boldsymbol{\Delta}(\mathbf{y})\, \mathrm{d}V_x\, \mathrm{d}V_y \right) , \tag{A2}$$

such that

$$\int \mathcal{D}\boldsymbol{\Delta}\, P[\boldsymbol{\Delta}] = 1 \,, \tag{A3}$$

where the integration is performed on the space of fluctuating fields $\boldsymbol{\Delta}(\mathbf{x})$. This means that the integral is evaluated over all possible functions $\boldsymbol{\Delta}(\mathbf{x})$, in an infinite dimensional space with the measure $\mathcal{D}\boldsymbol{\Delta}$. It is worthwhile noting that, path integrals can be evaluated in a closed form very rarely, however, in the case of Gaussian path integrals (the present case) exact calculations can be performed. In fact, after defining $P[\boldsymbol{\Delta}]$, the correlation tensor can be written as

$$\mathbf{C}_\lambda(\mathbf{x},\mathbf{y}) = \langle \mathbf{\Delta}(\mathbf{x}) \otimes \mathbf{\Delta}(\mathbf{y})^\dagger \rangle = \int \mathcal{D}\mathbf{\Delta}\, \mathbf{\Delta} \otimes \mathbf{\Delta}^\dagger\, P[\mathbf{\Delta}] \tag{A4}$$
$$= \frac{1}{Z} \int \mathcal{D}\mathbf{\Delta}\, \mathbf{\Delta} \otimes \mathbf{\Delta}^\dagger \exp\left(-\frac{1}{2k_B} \int_V \int_V \mathbf{\Delta}(\mathbf{x})^\dagger \mathcal{H}_\lambda(\mathbf{x},\mathbf{y})\, \mathbf{\Delta}(\mathbf{y})\, \mathrm{d}V_x\, \mathrm{d}V_y \right) ,$$

and, the evaluation of the path integrals reduce to

$$\mathbf{C}_\lambda(\mathbf{x},\mathbf{y}) = k_B \mathcal{H}_\lambda^{-1}(\mathbf{x},\mathbf{y}) , \tag{A5}$$

where $\mathcal{H}_\lambda^{-1}$ is the inverse of the operator $\mathcal{H}_\lambda$, *i.e.* the Green's functions which satisfy

$$\int \mathcal{H}_\lambda^{-1}(\mathbf{x},\mathbf{z})\; \mathcal{H}_\lambda(\mathbf{z},\mathbf{y})\; \mathrm{d}V_{\mathbf{z}} = \mathcal{I}\delta(\mathbf{x}-\mathbf{y}) , \tag{A6}$$

with $\mathcal{I}$ the 5×5 identity matrix. The complete derivation of the above results can be found in[57], here it is worth describing the strong analogy with the finite-dimensional case of Gaussian integrals. In fact, the correlation deduced from a Gaussian path integral (see Eq. A5) is formally equivalent to the covariance matrix in multidimensional Gaussian distribution. For a multidimensional Gaussian process $\mathbf{W} \in \mathbb{R}^N$ with probability density

$$P[\mathbf{W}] = \frac{1}{\sqrt{(2\pi \mathrm{det}\mathbf{H^{-1}})^N}} \exp\left(-\frac{1}{2}\mathbf{W}^T\mathbf{H}\mathbf{W} \right) , \tag{A7}$$

it is well-known that the covariance matrix $\mathbf{C} = \langle \mathbf{W} \otimes \mathbf{W}^T \rangle = \mathbf{H}^{-1}$. Under this respect, the expression given in Eq. A5 is the infinite-dimensional extension of the above result[62].

Given the expression for $\mathcal{H}$ in Eq. (13), Eq. (A6) takes the form

$$\left(\frac{c_{T0}^2}{T_0\rho_0} - \frac{\lambda}{T_0}\nabla_{\mathbf{x}}^2 \right) C_{\lambda 11}(\mathbf{x},\mathbf{y}) = k_B\delta(\mathbf{x}-\mathbf{y}) , \tag{A8}$$

$$\frac{\rho_0}{T_0}\, \mathbf{C}_{\lambda 22}(\mathbf{x},\mathbf{y}) = k_B \mathbf{I}\delta(\mathbf{x}-\mathbf{y}) , \tag{A9}$$

$$\frac{\rho_0 c_{v0}}{T_0^2}\, C_{\lambda 33}(\mathbf{x},\mathbf{y}) = k_B\delta(\mathbf{x}-\mathbf{y}) , \tag{A10}$$

where $C_{\lambda 11}$, $\mathbf{C}_{\lambda 22}$ and $C_{\lambda 33}$ are the correlations for density, velocity and temperature fluctuation fields. Furthermore, the translational symmetry implies $\mathbf{C}_\lambda(\mathbf{x},\mathbf{y}) = \mathbf{C}_\lambda(\mathbf{x}-\mathbf{y})$. The Eq.s (A9, A10) can be easily solved to identify

$$\mathbf{C}_{\lambda 22}\left(\mathbf{x}-\mathbf{y}\right) = \langle \tilde{\mathbf{v}}(\mathbf{x}) \otimes \tilde{\mathbf{v}}(\mathbf{y}) \rangle = \frac{k_B T_0}{\rho_0}\, \mathbf{I}\delta\left(\mathbf{x}-\mathbf{y}\right) , \tag{A11}$$

$$C_{\lambda 33}\left(\mathbf{x}-\mathbf{y}\right) = \langle \tilde{T}(\mathbf{x})\tilde{T}(\mathbf{y}) \rangle = \frac{k_B T_0^2}{\rho_0 c_{v0}}\delta\left(\mathbf{x}-\mathbf{y}\right) . \tag{A12}$$

In order to determine the density correlation function $C_{\lambda 11}(\mathbf{x}-\mathbf{y}) = \langle \tilde{\rho}(\mathbf{x})\tilde{\rho}(\mathbf{y}) \rangle$ it is instrumental to introduce the Fourier transform of the density correlation

$$\hat{\tilde{\rho}}(\mathbf{k}) = \int \tilde{\rho}(\mathbf{x}) \exp\left(-i\,\mathbf{k}\cdot\mathbf{x}\right)\, \mathrm{d}V_{\mathbf{x}} , \tag{A13}$$

so that $\hat{C}_{\lambda 11}(\mathbf{k}) = \langle \hat{\tilde{\rho}}(\mathbf{k})\hat{\tilde{\rho}}(-\mathbf{k}) \rangle$, and Eq. (A8) is transformed in an algebraic equation in the Fourier space as

$$\left(\frac{c_{T0}^2}{T_0\rho_0} + \frac{\lambda}{T_0}|\mathbf{k}|^2 \right) \hat{C}_{\lambda 11}(\mathbf{k}) = k_B , \tag{A14}$$

implying that

$$\hat{C}_{\lambda 11}(\mathbf{k}) = \frac{k_B T_0 \rho_0}{c_{T0}^2 + \rho_0\lambda|\mathbf{k}|^2} , \tag{A15}$$

which is known as *structure factor* of the fluid. The density fluctuation correlation in the physical space is then identified as the inverse Fourier transform of the structure factor

$$C_{\lambda 11}(\mathbf{x}-\mathbf{y}) = \frac{1}{(2\pi)^3} \int \hat{C}_{\lambda 11}(\mathbf{k}) \exp\left(i\,\mathbf{k}\cdot|\mathbf{x}-\mathbf{y}|\right) \mathrm{d}V_{\mathbf{k}}$$
$$= \frac{\mathrm{k}_B T_0}{4\pi\lambda\,|\mathbf{x}-\mathbf{y}|} \exp\left(-|\mathbf{x}-\mathbf{y}| \sqrt{\frac{c_{T0}^2}{\rho_0\lambda}} \right) . \tag{A16}$$

It is worth noting that $\hat{C}_{011}(\mathbf{k})$ is obtained from the SGT prediction of $\hat{C}_{\lambda 11}(\mathbf{k})$ as $|\mathbf{k}|^2 \to 0$.

REFERENCES

[1] Albert Einstein. *Investigations on the Theory of the Brownian Movement*. Courier Corporation, 1956.

[2] Ronald Forrest Fox and George E Uhlenbeck. Contributions to non-equilibrium thermodynamics. i. theory of hydrodynamical fluctuations. *Physics of Fluids (1958-1988)*, 13(8):1893–1902, 1970.

[3] Raymond D Mountain. Spectral distribution of scattered light in a simple fluid. *Reviews of Modern Physics*, 38(1):205, 1966.

[4] Dieter Forster. *Hydrodynamic fluctuations, broken symmetry, and correlation functions*. CRC Press, 2018.

[5] Jose M Ortiz De Zarate and Jan V Sengers. *Hydrodynamic fluctuations in fluids and fluid mixtures*. Elsevier, 2006.

[6] Hans Christian Öttinger and Miroslav Grmela. Dynamics and thermodynamics of complex fluids. ii. illustrations of a general formalism. *Physical Review E*, 56(6):6633, 1997.

[7] Pep Español, Jesús G Anero, and Ignacio Zúñiga. Microscopic derivation of discrete hydrodynamics. *The Journal of chemical physics*, 131(24):244117, 2009.

[8] Pep Español. Stochastic differential equations for non-linear hydrodynamics. *Physica A: Statistical Mechanics and its Applications*, 248(1-2):77–96, 1998.

[9] Diego Camargo, JA de La Torre, D Duque-Zumajo, Pep Español, Rafael Delgado-Buscalioni, and Farid Chejne. Nanoscale hydrodynamics near solids. *The Journal of Chemical Physics*, 148(6):064107, 2018.

[10] D Duque-Zumajo, Diego Camargo, JA de La Torre, Farid Chejne, and Pep Español. Discrete hydrodynamics near solid planar walls. *Physical Review E*, 99(5):052130, 2019.

[11] Aleksandar Donev, Eric Vanden-Eijnden, Alejandro Garcia, and John Bell. On the accuracy of finite-volume schemes for fluctuating hydrodynamics. *Communications in Applied Mathematics and Computational Science*, 5(2):149–197, 2010.

[12] Steven Delong, Boyce E Griffith, Eric Vanden-Eijnden, and Aleksandar Donev. Temporal integrators for fluctuating hydrodynamics. *Physical Review E*, 87(3):033302, 2013.

[13] Florencio Balboa, John B Bell, Rafael Delgado-Buscalioni, Aleksandar Donev, Thomas G Fai, Boyce E Griffith, and Charles S Peskin. Staggered schemes for fluctuating hydrodynamics. *Multiscale Modeling & Simulation*, 10(4):1369–1408, 2012.

[14] Aleksandar Donev, Andy Nonaka, Yifei Sun, Thomas Fai, Alejandro Garcia, and John Bell. Low mach number fluctuating hydrodynamics of diffusively mixing fluids. *Communications in Applied Mathematics and Computational Science*, 9(1):47–105, 2014.

[15] Antonio Russo, Sergio P Perez, Miguel A Durán-Olivencia, Peter Yatsyshin, José A Carrillo, and Serafim Kalliadasis. A finite-volume method for fluctuating dynamical density functional theory. *Journal of Computational Physics*, 428:109796, 2021.

[16] Francesco Magaletti, Mirko Gallo, Sergio P Perez, José A Carrillo, and Serafim Kalliadasis. A positivity-preserving scheme for fluctuating hydrodynamics. *Journal of Computational Physics*, 463:111248, 2022.

[17] Bruce J Berne and Robert Pecora. *Dynamic light scattering: with applications to chemistry, biology, and physics*. Courier Corporation, 2000.

[18] François Detcheverry and Lydéric Bocquet. Thermal fluctuations in nanofluidic transport. *Physical review letters*, 109(2):024501, 2012.

[19] Chengxi Zhao, James E Sprittles, and Duncan A Lockerby. Revisiting the rayleigh–plateau instability for the nanoscale. *Journal of Fluid Mechanics*, 861, 2019.

[20] Yixin Zhang, James E Sprittles, and Duncan A Lockerby. Thermal capillary wave growth and surface roughening of nanoscale liquid films. *Journal of Fluid Mechanics*, 915, 2021.

[21] Chengxi Zhao, Jiayi Zhao, Ting Si, and Shuo Chen. Influence of thermal fluctuations on nanoscale free-surface flows: A many-body dissipative particle dynamics study. *Physics of Fluids*, 33(11):112004, 2021.

[22] Ting Ye, Dingyi Pan, Can Huang, and Moubin Liu. Smoothed particle hydrodynamics (sph) for complex fluid flows: Recent developments in methodology and applications. *Physics of Fluids*, 31(1):011301, 2019.

[23] Sho C Takatori and Amaresh Sahu. Active contact forces drive nonequilibrium fluctuations in membrane vesicles. *Physical Review Letters*, 124(15):158102, 2020.

[24] Ludger Johannes, Weria Pezeshkian, John H Ipsen, and Julian C Shillcock. Clustering on membranes: fluctuations and more. *Trends in cell biology*, 28(5):405–415, 2018.

[25] Michael J Skaug, Christian Schwemmer, Stefan Fringes, Colin D Rawlings, and Armin W Knoll. Nanofluidic rocking brownian motors. *Science*, 359(6383):1505–1508, 2018.

[26] Changho Kim, Andy Nonaka, John B Bell, Alejandro L Garcia, and Aleksandar Donev. Fluctuating hydrodynamics of reactive liquid mixtures. *The Journal of chemical physics*, 149(8):084113, 2018.

[27] Aleksandar Donev, Andrew J Nonaka, Changho Kim, Alejandro L Garcia, and John B Bell. Fluctuating hydrodynamics of electrolytes at electroneutral scales. *Physical Review Fluids*, 4(4):043701, 2019.

[28] Mirko Gallo, Francesco Magaletti, Davide Cocco, and Carlo Massimo Casciola. Nucleation and growth dynamics of vapour bubbles. *Journal of Fluid Mechanics*, 883, 2020.

[29] Alberto Vailati and Marzio Giglio. Giant fluctuations in a free diffusion process. *Nature*, 390(6657):262–265, 1997.

[30] Dmytro Bandak, Nigel Goldenfeld, Alexei A Mailybaev, and Gregory Eyink. Dissipation-range fluid turbulence and thermal noise. *Physical Review E*, 105(6):065113, 2022.

[31] John B Bell, Andrew Nonaka, Alejandro L Garcia, and Gregory Eyink. Thermal fluctuations in the dissipation range of homogeneous isotropic turbulence. *Journal of Fluid Mechanics*, 939, 2022.

[32] Dmytro Bandak, Gregory L Eyink, Alexei Mailybaev, and Nigel Goldenfeld. Thermal noise competes with turbulent fluctuations below millimeter scales. *arXiv preprint arXiv:2107.03184*, 2021.

[33] Ryan M McMullen, Michael C Krygier, John R Torczynski, and Michael A Gallis. Navier-stokes equations do not describe the smallest scales of turbulence in gases. *Physical Review Letters*, 128(11):114501, 2022.

[34] Detlef Lohse and Andrea Prosperetti. Homogeneous nucleation: Patching the way from the macroscopic to the nanoscopic description. *Proceedings of the National Academy of Sciences*, 113(48):13549–13550, 2016.

[35] Mirko Gallo, Francesco Magaletti, Dario Abbondanza, and Carlo Massimo Casciola. Vapor nucleation in metastable liquids: the continuum description. In *The Surface Wettability Effect on Phase Change*, pages 343–385. Springer, 2022.

[36] D Kashchiev and GM Van Rosmalen. Review: nucleation in solutions revisited. *Crystal Research and Technology*, 38(7-8):555–574, 2003.

[37] Johannes Diederik Van der Waals. The thermodynamic theory of capillarity under the hypothesis of a continuous variation of density. *Journal of Statistical Physics*, 20(2):200–244, 1979.

[38] Francesco Magaletti, Mirko Gallo, Luca Marino, and Carlo Massimo Casciola. Shock-induced collapse of a vapor nanobubble near solid boundaries. *International Journal of Multiphase Flow*, 84:34–45, 2016.

[39] James F Lutsko. Recent developments in classical density functional theory. *Advances in chemical physics*, 144:1, 2010.

[40] James F Lutsko. Density functional theory of inhomogeneous liquids. iv. squared-gradient approximation and classical nucleation theory. *The Journal of chemical physics*, 134(16):164501, 2011.

[41] Mirko Gallo, Francesco Magaletti, and Carlo Massimo Casciola. Heterogeneous bubble nucleation dynamics. *Journal of Fluid Mechanics*, 906, 2021.

[42] Mirko Gallo, Francesco Magaletti, and Carlo Massimo Casciola. Fluctuating hydrodynamics as a tool to investigate nucleation of cavitation bubbles. *Multiphase Flow: Theory and Applications*, page 347, 2018.

[43] Frédéric Caupin. Liquid-vapor interface, cavitation, and the phase diagram of water. *Physical Review E*, 71(5):051605, 2005.

[44] Francesco Magaletti, Mirko Gallo, and Carlo Massimo Casciola. Water cavitation from ambient to high temperatures. *Scientific reports*, 11(1):1–10, 2021.

[45] Øivind Wilhelmsen, Thuat T Trinh, Signe Kjelstrup, and Dick Bedeaux. Influence of curvature on the transfer coefficients for evaporation and condensation of lennard-jones fluid from square-gradient theory and nonequilibrium molecular dynamics. *The Journal of Physical Chemistry C*, 119(15):8160–8173, 2015.

[46] ES Benilov. Can a liquid drop on a substrate be in equilibrium with saturated vapor? *Physical Review E*, 104(3):L032103, 2021.

[47] ES Benilov. Capillary condensation of saturated vapor in a corner formed by two intersecting walls. *Physics of Fluids*, 34(6):062103, 2022.

[48] Francesco Magaletti, Anastasios Georgoulas, and Marco Marengo. Unraveling low nucleation temperatures in pool boiling through fluctuating hydrodynamics simulations. *International Journal of Multiphase Flow*, 130:103356, 2020.

[49] Francesco Magaletti, Mirko Gallo, Luca Marino, and Carlo Massimo Casciola. Dynamics of a vapor nanobubble collapsing near a solid boundary. In *Journal of Physics: Conference Series*, volume 656, page 012012. IOP Publishing, 2015.

[50] Dario Abbondanza, Mirko Gallo, and Carlo Massimo Casciola. Cavitation over solid surfaces: microbubble collapse, shock waves, and elastic response. *Meccanica*, pages 1–11, 2022.

[51] ES Benilov. Dynamics of a drop floating in vapor of the same fluid. *Physics of Fluids*, 34(4):042104, 2022.

[52] ES Benilov. The dynamics of liquid films, as described by the diffuse-interface model. *Physics of Fluids*, 32(11):112103, 2020.

[53] Matteo Bottacchiari, Mirko Gallo, Marco Bussoletti, and Carlo Massimo Casciola. Activation energy and force fields during topological transitions of fluid lipid vesicles. *Communications Physics*, 5(1):1–12, 2022.

[54] Mukul D Tikekar, Kris T Delaney, Michael C Villet, Douglas R Tree, and Glenn H Fredrickson. A phase field model for dynamic simulations of reactive blending of polymers. *Soft Matter*, 18(4):877–893, 2022.

[55] Barry Z Shang, Nikolaos K Voulgarakis, and Jhih-Wei Chu. Fluctuating hydrodynamics for multiscale simulation of inhomogeneous fluids: Mapping all-atom molecular dynamics to capillary waves. *The Journal of chemical physics*, 135(4):044111, 2011.

[56] Anuj Chaudhri, John B Bell, Alejandro L Garcia, and Aleksandar Donev. Modeling multiphase flow using fluctuating hydrodynamics. *Physical Review E*, 90(3):033014, 2014.

[57] Mirko Gallo, Francesco Magaletti, and Carlo Massimo Casciola. Thermally activated vapor bubble nucleation: The landau-lifshitz–van der waals approach. *Physical Review Fluids*, 3(5):053604, 2018.

[58] Mirko Gallo, Francesco Magaletti, and Carlo M Casciola. Phase field/fluctuating hydrodynamics approach for bubble nucleation. In *THMT-18. Turbulence Heat and Mass Transfer 9 Proceedings of the Ninth International Symposium On Turbulence Heat and Mass Transfer*. Begel House Inc., 2018.

[59] J Karl Johnson, John A Zollweg, and Keith E Gubbins. The lennard-jones equation of state revisited. *Molecular Physics*, 78(3):591–618, 1993.

[60] Vincent K Shen and Pablo G Debenedetti. A kinetic theory of homogeneous bubble nucleation. *The Journal of chemical physics*, 118(2):768–783, 2003.

[61] Nigel Goldenfeld. *Lectures on phase transitions and the renormalization group*. CRC Press, 2018.

[62] Carson C Chow and Michael A Buice. Path integral methods for stochastic differential equations. *The Journal of Mathematical Neuroscience (JMN)*, 5(1):8, 2015.

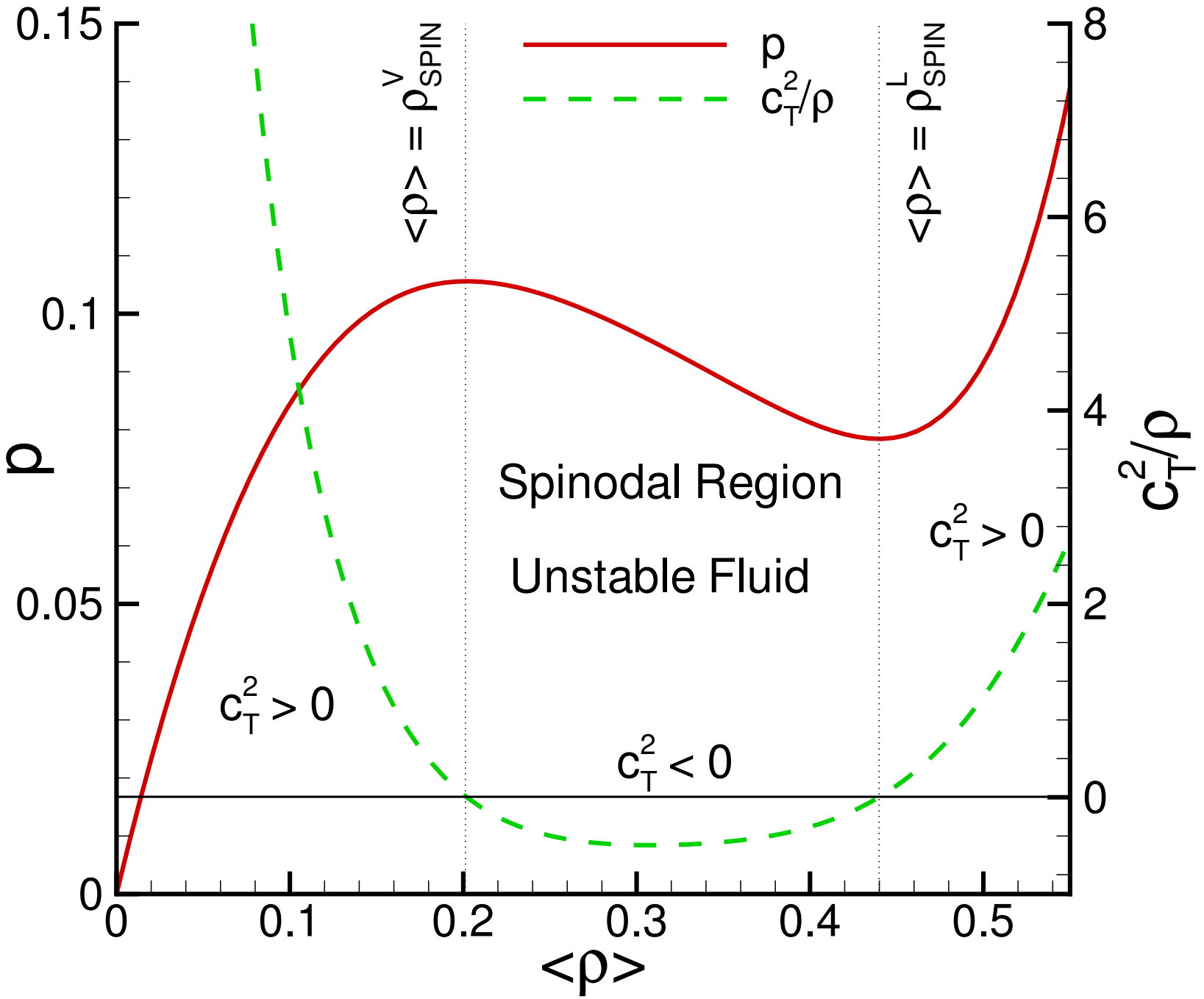
0.15
0.1
0.05
0
p
0
0.1
0.2
0.3
0.4
0.5
<ρ>
8
6
4
2
0
c_T^2/ρ
p
c_T^2/ρ
<ρ> = ρ_SPIN^V
<ρ> = ρ_SPIN^L
Spinodal Region
Unstable Fluid
c_T^2 > 0
c_T^2 < 0
c_T^2 > 0

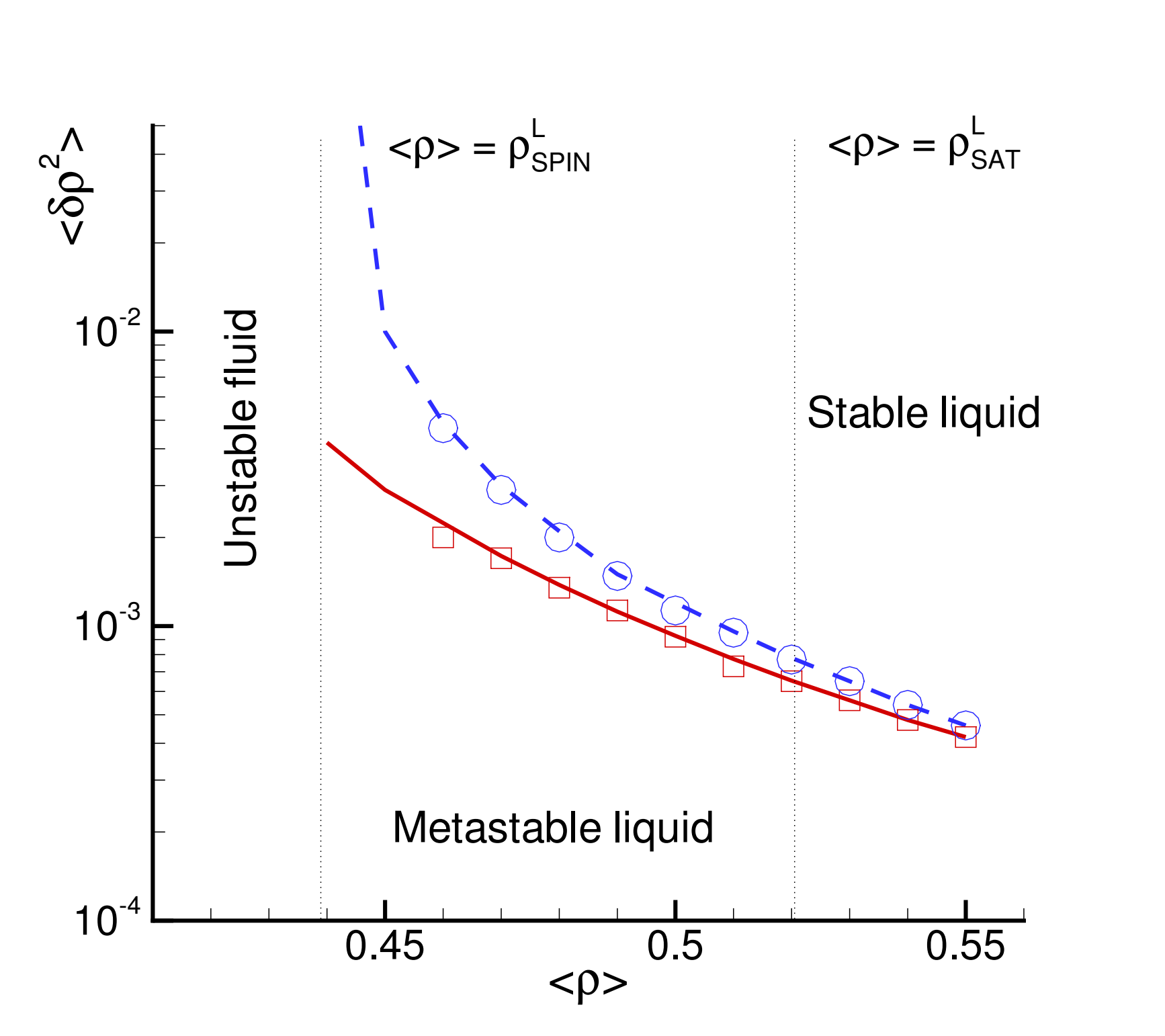
$\langle\delta\rho^2\rangle$
10^{-2}
10^{-3}
10^{-4}
$\langle\rho\rangle = \rho^L_{SPIN}$
$\langle\rho\rangle = \rho^L_{SAT}$
Unstable fluid
Stable liquid
Metastable liquid
0.45
0.5
0.55
$\langle\rho\rangle$

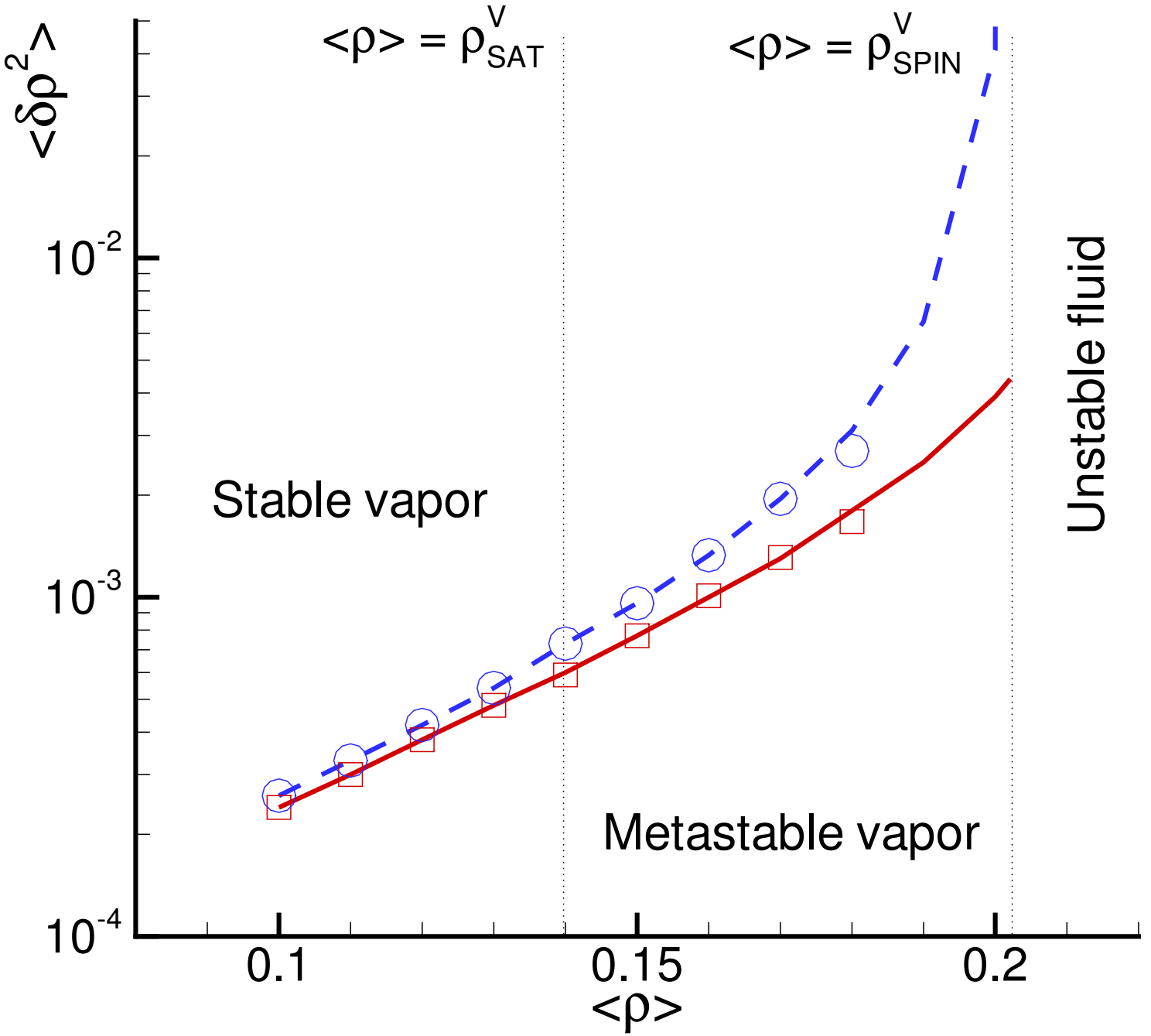
$\langle\rho\rangle = \rho^{V}_{SAT}$
$\langle\rho\rangle = \rho^{V}_{SPIN}$
$\langle\delta\rho^2\rangle$
10^{-2}
10^{-3}
10^{-4}
Stable vapor
Metastable vapor
Unstable fluid
0.1
0.15
0.2
$\langle\rho\rangle$

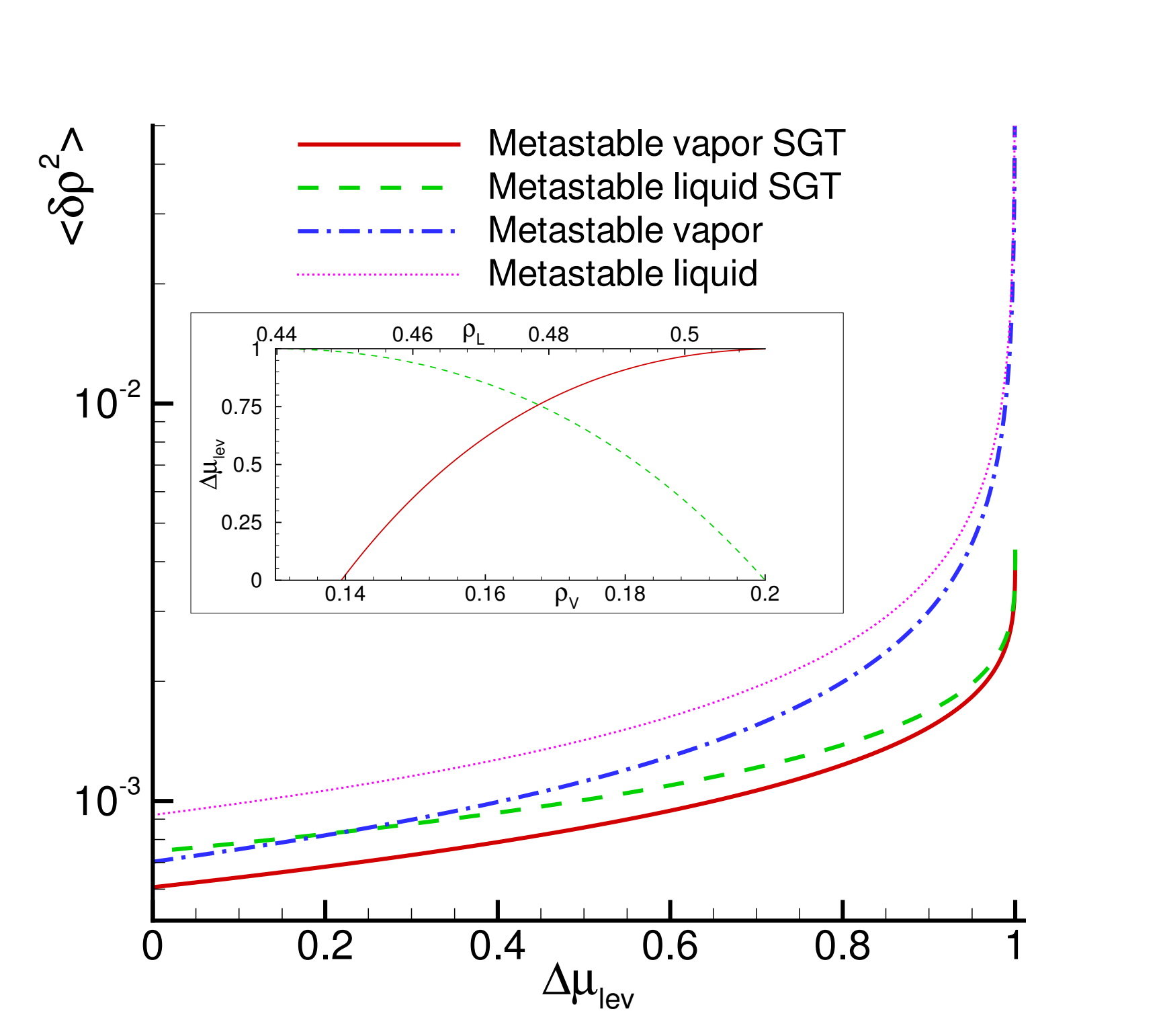
Metastable vapor SGT
Metastable liquid SGT
Metastable vapor
Metastable liquid
$<\delta\rho^2>$
10^{-2}
10^{-3}
0
0.2
0.4
0.6
0.8
1
$\Delta\mu_{lev}$
0.44
0.46
ρ_L
0.48
0.5
1
0.75
0.5
0.25
0
$\Delta\mu_{lev}$
0.14
0.16
ρ_V
0.18
0.2

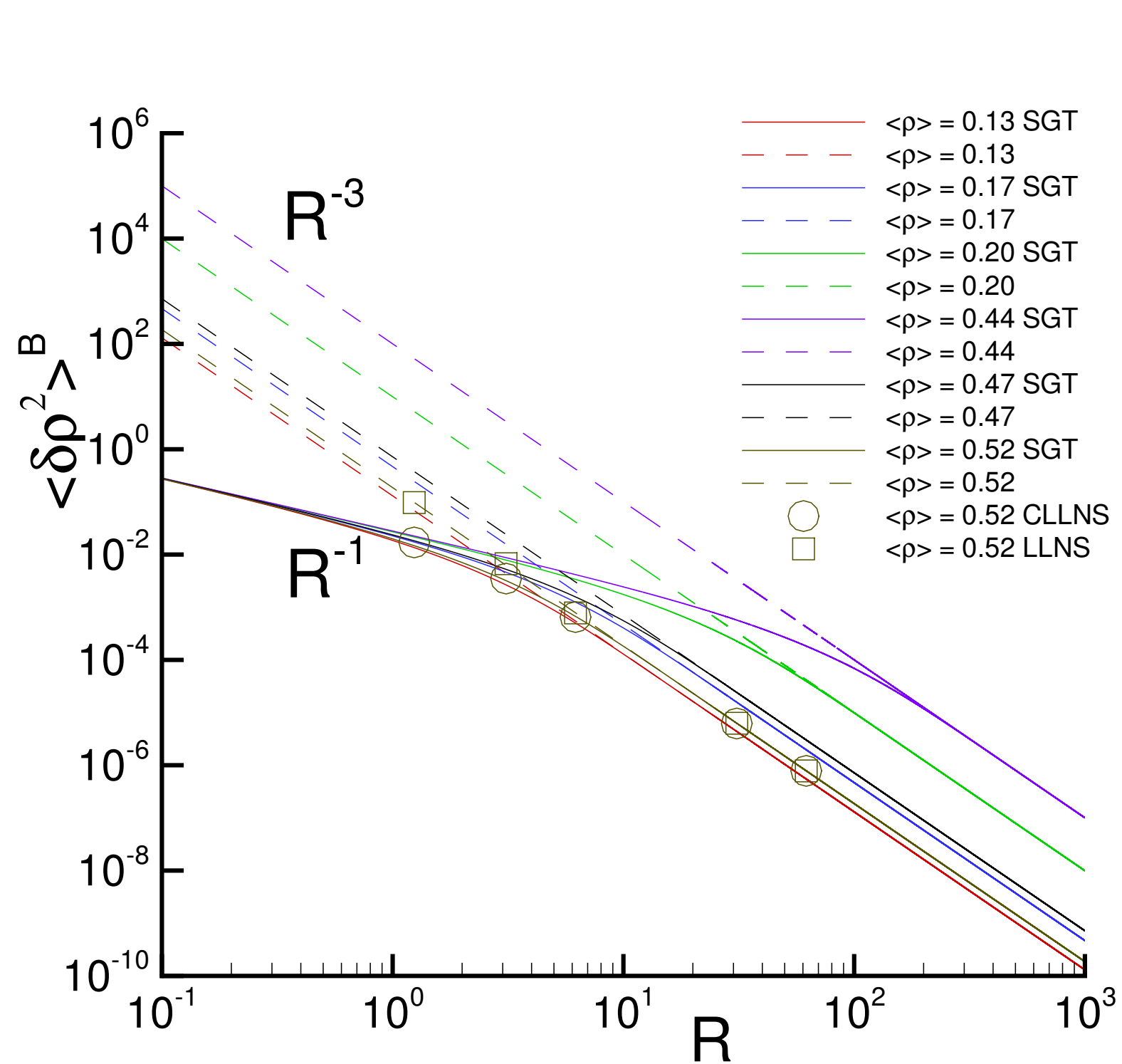
10^6
10^4
10^2
10^0
10^{-2}
10^{-4}
10^{-6}
10^{-8}
10^{-10}
10^{-1}
10^0
10^1
10^2
10^3
R
$<\delta\rho^2>^B$
R^{-3}
R^{-1}
<ρ> = 0.13 SGT
<ρ> = 0.13
<ρ> = 0.17 SGT
<ρ> = 0.17
<ρ> = 0.20 SGT
<ρ> = 0.20
<ρ> = 0.44 SGT
<ρ> = 0.44
<ρ> = 0.47 SGT
<ρ> = 0.47
<ρ> = 0.52 SGT
<ρ> = 0.52
<ρ> = 0.52 CLLNS
<ρ> = 0.52 LLNS

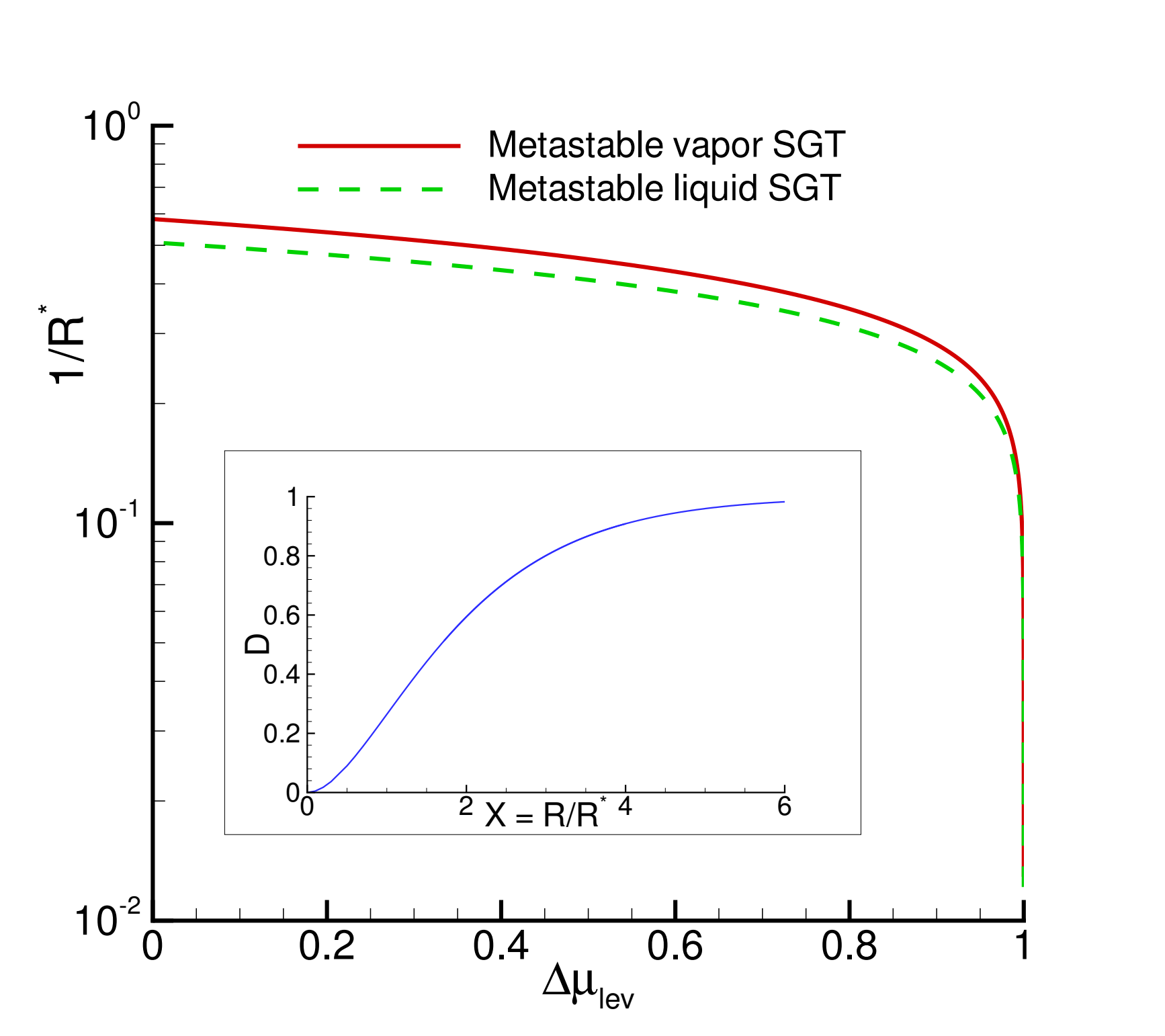
Metastable vapor SGT
Metastable liquid SGT
1/R*
Δμlev
D
X = R/R*
10^0
10^-1
10^-2
0
0.2
0.4
0.6
0.8
1
2
4
6